Available online at www.sciencedirect.com
SCIENCE DIRECT®
Surface Science 545 (2003) 19–33
SURFACE SCIENCE
www.elsevier.com/locate/susc

Reaction of atomic oxygen with a Pt(1 1 1) surface: chemical and structural determination using XPS, CAICISS and LEED

C.R. Parkinson *, M. Walker, C.F. McConville *

Department of Physics, University of Warwick, Gibbet Hill Road, Coventry CV4 7AL, UK

Received 23 June 2003; accepted for publication 8 August 2003

Abstract

The adsorption of thermally cracked atomic oxygen on the Pt(1 1 1) surface has been investigated using X-ray photoelectron spectroscopy (XPS), co-axial impact collision ion scattering spectroscopy (CAICISS), and low energy electron diffraction (LEED). High concentrations of atomic oxygen ($\sim 2\times10^{15}$ atoms cm^{-2}) can be cleanly adsorbed on the Pt(1 1 1) surface at room temperature by dosing the surface with externally generated atomic oxygen at relatively low exposures ($\sim$50 L). Two states of oxygen are readily resolved by XPS with O 1s binding energies at 530.8 and 530.2 eV. These states are assigned to chemisorbed oxygen and to an oxidic oxygen state, respectively. XPS spectra of the Pt 4f region confirm the existence of an oxide species with the appearance of a peak at 2.4 eV higher binding energy than the bulk Pt $4f_{5/2}$ peak. Using a combination of angle-resolved XPS, CAICISS, and LEED, evidence is provided to suggest that penetration of oxygen into the surface occurs most likely by an exchange mechanism resulting in the reconstruction of the Pt atoms in the first two atomic layers. On annealing the oxygen covered surface at 500 °C the oxidic layer is observed to decompose and a p(2×2)-O reconstruction is observed. A CAICISS study of this reconstructed surface presents evidence in favour of O atoms occupying h.c.p. sites over f.c.c. sites. Low exposures ($\sim$5 L) of atomic oxygen result in a sharp p(2×2) reconstruction of the Pt(1 1 1) surface and a single species in the O 1s spectrum at a binding energy of 530.8 eV. Both the p(2×2)-O overlayer and the oxide species are shown to be extremely sensitive to the electron and ion beam.

Keywords: Chemisorption; Oxidation; Oxygen; Platinum; X-ray photoelectron spectroscopy; Low energy electron diffraction (LEED); Low energy ion scattering (LEIS)

1. Introduction

The adsorption of molecular oxygen on the Pt(1 1 1) surface has been studied extensively over many years [1,3–17,25–28]. In particular, research into the platinum oxide system has been motivated by the importance of Pt in several catalytic heterogeneous oxidation reactions [2,3], and fundamentally from a desire to understand the physical

* Corresponding authors. Tel.: +44-24-7657-4034; fax: +44-24-7669-2016 (C.R. Parkinson), Tel.: +44-24-7652-4236; fax: +44-24-7669-2016 (C.F. McConville).

E-mail addresses: c.parkinson@warwick.ac.uk (C.R. Parkinson), c.f.mcconville@warwick.ac.uk (C.F. McConville).

0039-6028/$ - see front matter © 2003 Elsevier B.V. All rights reserved.
doi:10.1016/j.susc.2003.08.029

and chemical interactions of oxygen with the surfaces of Group VIII metals.

Studies of the adsorption of molecular oxygen on the Pt(1 1 1) surface have yielded consistent results. Gland et al. [4,5] first investigated this system using low energy electron diffraction (LEED), ultra-violet photoelectron spectroscopy (UPS), electron energy loss spectroscopy (EELS) and temperature programmed desorption (TPD). They identified the existence of a molecular species, which dissociated into a chemisorbed state above 150 K. Since then many spectroscopic techniques have also been applied to characterise the different adsorption phases of oxygen on Pt under different conditions. Photoemission spectroscopy [6,7,9], TPD [7,10], near edge X-ray adsorption spectroscopy (NEXAFS) [11], LEED [8,26–28], and EELS studies [7,9] have identified and characterised a physisorbed state, two chemisorbed molecular states, and, via a thermally activated molecular precursor, a chemisorbed atomic state that forms an ordered overlayer with a p(2×2) LEED pattern. For this latter chemisorbed state a saturation coverage of 0.25 ML ($\sim 3.8\times10^{14}$ atoms cm^{-2}) was observed [1,3–11].

Coverages of adsorbed O greater than 0.25 ML have also been observed however, the results of these studies have been much less consistent. Gland [5] and Steininger et al. [10] both found that the maximum possible surface coverage of adsorbed O could be enhanced by a factor of two following exposure to an electron beam. Dahlgren and Hemminger [12] also observed an enhanced oxygen coverage following exposure to, and decomposition of, NO_2. Furthermore, Derry and Ross [9] observed that a combination of high surface temperature and high O_2 pressures ($\sim10^{-3}$ Pa) resulted in a three to fivefold increase in the saturation coverage of oxygen. Using different techniques these groups concluded that these high oxygen concentration states are chemically identical to those observed at low oxygen concentrations, and furthermore that the oxygen appears to reside on the surface with no significant penetration into the bulk, as would be characterised by oxidation. In a number of investigations the formation of a further oxygen state has been claimed [4,13,15], a so-called ''non-reactive dissolved oxygen'' or ''sub-surface oxide'' state that could be formed at 700 °C at low oxygen pressures ($\sim10^{-3}$–10^{-5} Pa), and was shown to decompose above 900 °C. However, the formation of this surface Pt oxide is contentious since this species has been shown to be associated with impurities (Si or Ca) in the Pt crystals used [14,41].

Recently King and co-workers [16] proposed that there is a critical coverage, θ_c^{thd}, at which the transition between the O chemisorbed phase and the appearance of an oxidic film occurs is thermodynamically, and not kinetically, determined. Below this critical coverage the heat of formation of the chemisorbed phase is higher than the heat of formation of the oxide. As the O coverage increases the repulsive interactions between the O adatoms drive the differential heat of adsorption down sharply until, at the critical coverage, it is equal to that of the formation of the oxide film. Furthermore, density functional calculations by Ganduglia-Pirovano and coworkers [17,18], addressing the initial incorporation of oxygen into the surfaces of Ru to Ag, found that the incorporation of oxygen into the surface region is initially less stable than on-surface chemisorption. This is understood to be due to the additional cost of distorting the substrate lattice and the breaking of metal bonds required for incorporation. However, with increasing surface coverage this preference is observed to decrease due to the repulsive interactions within the more densely packed electronegative O adlayer. As such, above certain coverage the occupation of the sub-surface sites becomes more favourable compared to continued filling of surface sites.

In this paper a study of a new high oxygen concentration state on the Pt(1 1 1) surface formed by exposing the Pt(1 1 1) surface to thermally cracked atomic oxygen at room temperature is presented. In addition the Pt(1 1 1) p(2×2)-O surface formed by either exposure to low doses of atomic oxygen or by annealing the new high oxygen concentrate state, has been investigated. X-ray photoelectron spectroscopy (XPS), co-axial impact collision ion scattering spectroscopy (CAICISS) and LEED have all been used to determine the chemical and structural properties of these surfaces.

2. Experimental

The experiments were carried out in a UHV chamber equipped with a retractable LEED optic (Omicron), a dual anode X-ray source (Vacuum Generators), a 100 mm concentric hemispherical electron analyser (VSW, HA100), and a *bolt-on* CAICISS system (described later). The main chamber is pumped by ion, diffusion, and titanium sublimation pumps, and has a nominal base pressure of $\approx 1\times10^{-10}$ mbar. The Pt(1 1 1) crystal (Metal Crystals and Oxides, UK) was mounted on the end of a manipulator capable of both polar and azimuthal rotation and sample heating. The sample temperature could be accurately controlled in the range 20–800 °C, by use of e-beam heating of the sample, which was monitored using a chromel–alumel thermocouple in close contact to the sample.

2.1. XPS analysis

The XPS spectra were taken using the Al K_α X-ray source of the dual anode and was operated at 200 W. The analyser was operated in the fixed analyser transmission mode and set at a pass energy of 25 eV. All binding energies were calibrated relative to the Pt $4f_{5/2}$ peak at 71.2 eV [19].

2.2. CAICISS

Over the last few years the surface structure of adsorbate–substrate systems has been investigated using coaxial impact collision ion scattering spectroscopy [20,21]. The technique utilises the fact that the scattering of low energy inert gas ions can be described in terms of simple binary collisions. From an analysis of the energy and flux of the scattered ion and neutral particles as a function of incidence or azimuthal angle it is possible to determine the chemical composition and structural arrangement of atoms at the surface with single layer sensitivity. A schematic of the CAICISS equipment used in these experiments is shown in Fig. 1. The modular CAICISS instrument at Warwick has been constructed such that pulses of ions are directed onto the sample through a hole in the centre of the detector. The ions which scatter off the surface at angles close to 180° are detected in a time-of-flight mode using a micro-channel plate detector. With reference to Fig. 1, low energy ions (He^+, 2–5 keV) are produced using an emission stabilised Nielson ion source [22]. The ions are extracted and focused, using an Einzel lens, before travelling along the flight path to the main chamber. The flight path includes, in order away from the ion source, a collimating aperture (Col), a set of vertical and horizontal electrostatic

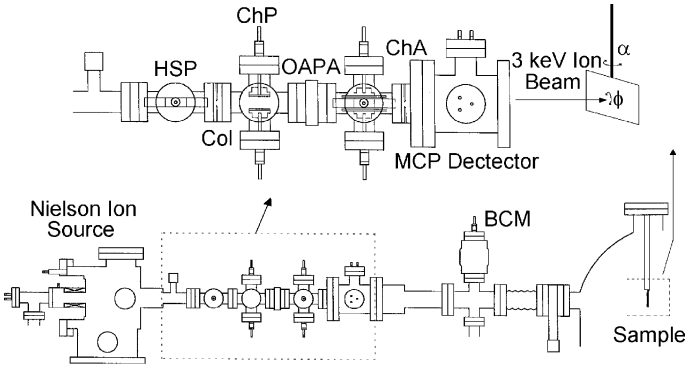

Fig. 1. The experimental arrangement of the Warwick modular CAICISS apparatus. The deflection plates and the collimating apertures are also shown in cross-section. Several components are labelled: MCP, micro-channel plate detector; OAPA, off-axis port aligner; ChP, chopping plates; ChA, chopping aperture; BCM, beam current monitor; HSP and VSP, horizontal and vertical steering plates; Col, collimator. The detector-to-sample separation is 80 cm. The scattering geometry adopted for the CAICISS experiments and the rotation axes for the incident polar (α) and azimuthal (Φ) angles are shown in the inset in the upper right.

deflection plates for electrostatic steering and chopping of the beam, an off-axis port aligner (OAPA) and a chopping aperture (ChA). The off-axis port aligner is utilised to induce a bend of 2° into the flight path to ensure that neutrals, produced by the ion source, fail to pass through the final aperture. Chopping of the beam was achieved using a fast rise time pulse applied to one set of the deflection plates (ChP) in order to sweep the beam across the final aperture. The resulting short pulses (~60 ns) then pass through an 8 mm hole in the centre of the micro-channel plate (MCP) detector (44 mm outside diameter) and down the remaining section of flight tube toward the sample. Back scattered ions and neutrals travel back down the flight tube, in which their energy differences cause them to be dispersed in time, before being detected in time-of-flight mode by the coaxially mounted micro-channel plate detector. All the data presented in this paper was obtained using an incident ion beam at an energy of 3 keV, produced from research grade helium. The scattering geometry and the axes defining the incidence angle α, and the azimuthal angle Φ are also shown in Fig. 1. Note that α is defined relative to the surface plane (rather than the surface normal), so in changing this angle from 0° to 180° the scattering geometry passes from grazing incidence, through to normal to the surface (90°) and back to grazing incidence from the opposite edge of the crystal. The azimuthal angle Φ, could be varied from −90° to +90°. Data acquisition was carried out using an EG&G Ortec MCB and Maestro II software. The polar rotation was automated with a stepping angle of 1.8° and an acquisition time at each step of 100 s.

Structural information has been obtained from the CAICISS spectra by measuring the intensities of the substrate scattering peaks as a function of incidence angle along the principal high symmetry azimuths as a function of surface oxidation. Data interpretation was aided by comparison with computer generated scattering simulations based on a series of trial surface structures. The simulations presented in this paper were generated using a simulation package (FAN) developed by Niehus [23]. The software computes the effect of shadowing and blocking by following the outgoing trajectories from a probed atom. For example, an atom in the surface region is chosen and an angular span of trajectories in all possible directions is computed around this atom, this calculation is the repeated for any number of atoms. For these calculations the principal input parameters are the atomic species, the ion species, the primary energy and the atomic coordinates. The principal purpose of these calculations is to provide a reasonably quantitative description of the effects of shadowing and blocking, and specifically of the critical features associated with these effects. For this reason, quantitative structure analysis concentrated on comparing the angles and relative intensities at which features occur in the experimental and theoretical results.

2.3. Sample preparation and dosing

The sample was cleaned following procedures described in detail elsewhere [24] and involved degassing and cycles of Ar^+ bombardment and extended annealing at 800 °C. Impurities such as Ca and Si have previously been suggested to the enhance oxidation of the Pt surface at high temperatures [1,14,15], but neither impurity was detected with XPS. The clean surface LEED pattern indicated a sharp (1×1) reconstruction. Dosing of atomic oxygen was achieved using a commercial molecular gas cracker (Oxford Applied Research, UK) which was mounted in direct line-of-site of the sample. Essentially, the thermal cracker consists of a W tube heated via electron bombardment and surrounded by a water-cooled casing. Dosing of atomic oxygen was carried out at room temperature, typically at pressures between 10^{-7} and 10^{-8} mbar, and the overall cracking efficiency of the source has been estimated to be 60% [25].

3. Results and discussion

3.1. LEED observations

A series of diffraction patterns, taken as a function of atomic oxygen exposure, are shown in Fig. 2. Image (2a) shows a sharp (1×1) pattern obtained from the clean Pt(1 1 1) surface. Image

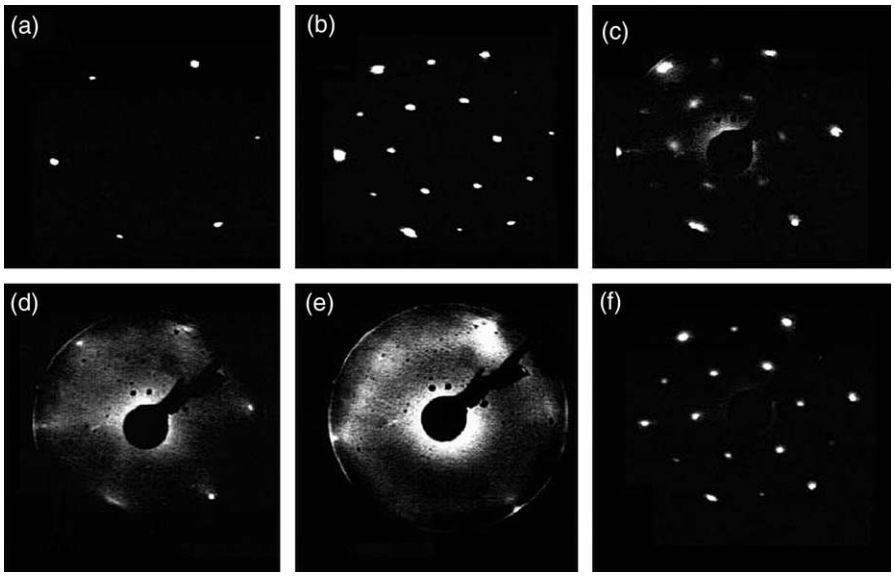

Fig. 2. LEED patterns taken as a function of atomic oxygen exposure for the clean Pt(1 1 1) surface at 84 eV (a), after a total exposure to 5 L (b), 10 L (c), 20 L (d) and 50 L (e) atomic oxygen at 25 °C. Pattern (f) was taken following annealing the surface at 500 °C.

(2b) shows the pattern obtained after exposing the surface to 5 L of atomic oxygen at 25 °C, and shows the surface is observed to reconstruct to a relatively sharp p(2×2) pattern. Such a pattern has previously been observed for oxygen on the Pt(1 1 1) surface and is characteristic of oxygen atoms adsorbed in threefold f.c.c. hollow sites [8,26–28]. Further exposure of the surface to atomic oxygen (total exposure of 10 L) at 25 °C leads to an increase in the background intensity of the LEED pattern, shown in image (2c). This increase may be an indication of an increase in the disorder of the adlayer or disruption of the Pt surface atoms. A faint (2×2) pattern can still be observed, albeit with poor contrast. Image (2d) shows the LEED pattern obtained after exposing the surface to a total of 20 L of atomic oxygen at 25 °C. The intensity of the background is observed to increase still further. More notably, streaks are now observed that appear to radiate from each of the (1×1) integral order spots, the intensity of which changed with electron energy but were not observed to coalesce into sharp spots. The streaks, observed before for oxygen on Au(1 1 1) [29], may indicate the onset of one-dimensional ordering or indicate that domains of p(2×2)-O–Pt superstructure are beginning to develop on the surface with increasing atomic oxygen exposure. LEED image (2e) shows that this streaking persists with increasing background intensity until saturation coverage appears to be reached (at a total exposure of 50 L), at which point, the substrate integral order spots are almost totally obscured by a high background intensity. This saturated surface was subsequently annealed, in stages, to 500 °C. Following annealing at 250 °C the background intensity was observed to reduce and the intensity of (1×1) spots increased. Compared with the clean surface the (1×1) spots were observed to be much broader. After annealing the surface at 400 °C a faint p(2×2) pattern began to emerge. This pattern became much stronger on further annealing, and became sharpest after annealing at 500 °C, as shown in image (2f).

The LEED images (2c) and (2d) are similar to those reported by Parker et al. [7] for NO_2 exposure on Pt(1 1 1) at 130 °C in respect that the half-order spots were also observed to decrease in intensity as a function of oxygen exposure. Parker et al. reported that a sharp p(2×2) pattern was formed for oxygen coverages less than 0.25 ML, and furthermore that the half-order spots persist at

higher oxygen coverages up to 0.75 ML, although with decreased contrast with respect to the background. Steininger et al. [10] reported that a diffuse p(2×2) diffraction pattern was observed for coverages up to 0.5 ML, with broader spots seen than for the 0.25 ML adlayer. They attributed this to a p(2×2) superstructure containing two oxygen atoms per unit cell, each occupying a threefold hollow site.

The increase in background intensity may also indicate some degree of surface disruption. Such features have been reported by Saliba et al. [29], and by Sault and Madix [30], for oxygen on Au(1 1 1) following exposure to ozone, and for oxygen on Au(1 1 0) following exposure to molecular oxygen, respectively, and have been ascribed to indicate the onset of a degree of disordering of the substrate. Further disruption of the surface is observed in this system on increasing the oxygen exposure until the substrate spots are no longer observed, a saturation dose (~50 L). However, on annealing the sample at 300 °C, intense (1×1) spots were observed to re-emerge, concomitant with a loss of the high background intensity. Furthermore, the appearance of a faint (2×2) pattern was also observed. Although it is possible that commensurate ordering of the adsorbate layer may be occurring, and resulting in the appearance of (1×1) spots at this temperature, it seems more likely that a reordering and or decomposition of the substrate layer occurs resulting in the reappearance of the Pt(1 1 1) surface (1×1) spots and a p(2×2) oxygen overlayer.

During the LEED experiments care was taken to minimise the time the oxygen-dosed sample was exposed the electron beam. Electron stimulated desorption of the oxygen overlayer was observed to proceed rapidly, over a matter of minutes. Since some perturbation of the Pt–O overlayer occurs during exposure to the LEED beam it is difficult to determine whether, and to what extent, the features observed in the LEED are due to either the Pt–O interaction or electron beam induced degradation.

3.2. XPS of the high oxygen concentration state

A series of XPS spectra were taken for the high oxygen concentration surface to determine whether the p(2×2)-O atomic state and the high oxygen concentration state are distinguishable, and therefore chemically different. Additionally, due to the quantitative nature of XPS, surface adatom concentrations were also determined (using quantification procedures which have been discussed elsewhere [31 and references therein]). Fig. 3 shows both the O 1s and Pt 4f XPS spectra for the clean Pt surface (3a), and the Pt surface following a saturation dose (50 L) of atomic oxygen at 25 °C (3b). Spectra obtained following subsequent annealing at 300 °C (3c), and at 500 °C (3d) for 20 min are also shown. Degradation of the O overlayer (in the form of oxygen loss from the surface) following XPS did not exceed 6%.

3.2.1. The O 1s spectra

Following the saturation exposure of atomic oxygen, the O 1s XPS spectra reveal an intense peak centred at a binding energy of 530.5 eV. This

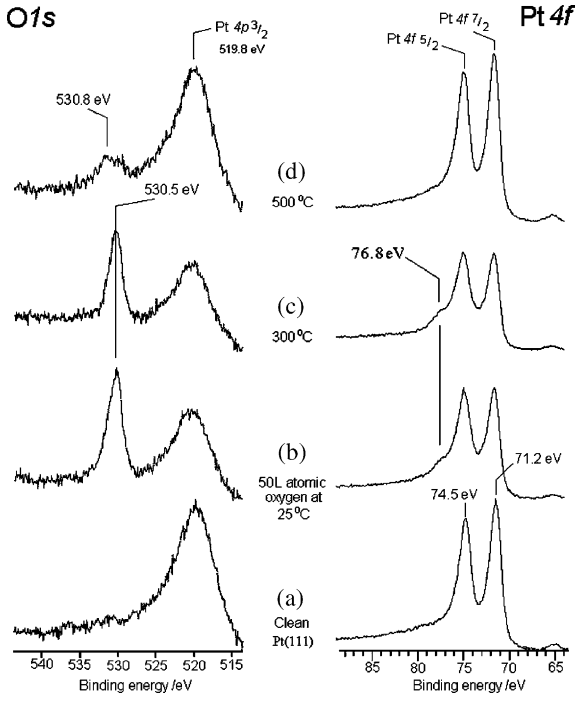

Fig. 3. O 1s and Pt 4f XPS spectra for the clean Pt surface (a), and the Pt surface following a saturation dose (50 L) of atomic oxygen at 25 °C (b), following subsequent annealing at 300 °C (c), and at 500 °C (d).

peak is slightly asymmetric on the high binding energy side, with a full width at half maximum (FWHM) of 2.3 eV. The concentration of O at the surface has been estimated to be 2×10^{15} atoms cm^{-2}. Due to the asymmetry exhibited by the peak and the slightly larger than expected FWHM, curve fitting analysis of the peak envelope was carried out. Initial fits using a Gaussian~Lorentzian mixture (70%:30%) suggested the presence of peaks at 530.2 and 530.8 eV with oxygen surface concentrations of 1.7×10^{15} and 3.4×10^{14} atoms cm^{-2} respectively. On annealing the sample at 300 °C for 20 min no detectable changes in the O 1s spectrum are observed. However, on further annealing at 500 °C complete loss of intensity at 530.2 eV is observed leaving only the O 1s peak at 530.8 eV. Since a p(2×2) LEED pattern was observed at this temperature during the LEED experiments, this O 1s species is assigned to an overlayer of atomic oxygen. The assignment of both O 1s binding energies will be discussed fully in Section 3.2.3.

3.2.2. The Pt 4f spectra

The Pt 4f XPS spectra also shown in Fig. 3, were taken at the same time as the O 1s spectra, following a saturation exposure of atomic oxygen. Spectrum (3b) reveals a shoulder on the high binding energy side of the Pt $4f_{5/2}$ peak at a binding energy of 76.8 eV; a positive shift in binding energy of 2.4 eV. In addition, changes in the relative intensities of the Pt $4f_{5/2}$ and $4f_{7/2}$ peaks are also observed. These features indicate the presence of additional structure hidden within the Pt $4f_{5/2}$ peak envelope. Following annealing at 300 °C no change in the Pt 4f peak envelope was observed, however, on further annealing at 500 °C, the Pt 4f peak envelope reverted back to that observed for the clean surface.

To better understand the characteristics of the Pt–O interaction, detailed curve fitting of the peaks in Pt region was carried out. Fig. 4 shows a curve fit of the Pt 4f surface core level spectra on exposure to 50 L of atomic oxygen at 25 °C. The clean metal spectrum was taken as a template for the detailed curve fitting. In Fig. 4 the bulk component Pt peaks are labelled I, and II while the shifted Pt peaks are labelled III, and IV. Quantification of the high binding energy shoulder, obtained from the intensity of the shifted Pt $4f_{5/2}$ peak, reveals a surface concentration of approximately 9.0×10^{14} atoms cm^{-2}. The shifted Pt $4f_{5/2}$ peak intensity was obtained by subtraction of a clean Pt $4f_{5/2}$ spectrum from the spectrum obtained after exposure to atomic oxygen. It is estimated that the concentrations derived from the XPS data are accurate to <10%.

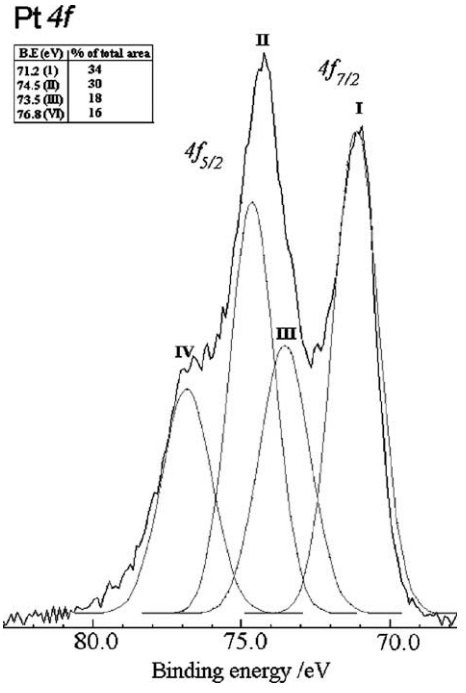

Fig. 4. A curve-fit of the Pt 4f surface core level spectra obtained following exposure of the clean Pt(1 1 1) surface to 50 L of atomic oxygen at 25 °C. The clean metal spectrum was taken as a template for the detailed curve fitting. Bulk component Pt peaks are labelled I, and II while the shifted Pt peaks are labelled III, and IV.

To investigate the high coverage oxygen species further XPS spectra were taken at a number of take-off angles to increase the relative surface sensitivity. Fig. 5 shows XPS spectra taken at normal emission (a), 45° (b) and 75° (c) off normal, whereby the latter is the most surface sensitive, as shown in the schematic inset. Between collecting spectra at each angle the surface was cleaned and re-exposed to a saturation dose of atomic oxygen in an effort to negate adlayer degradation by the

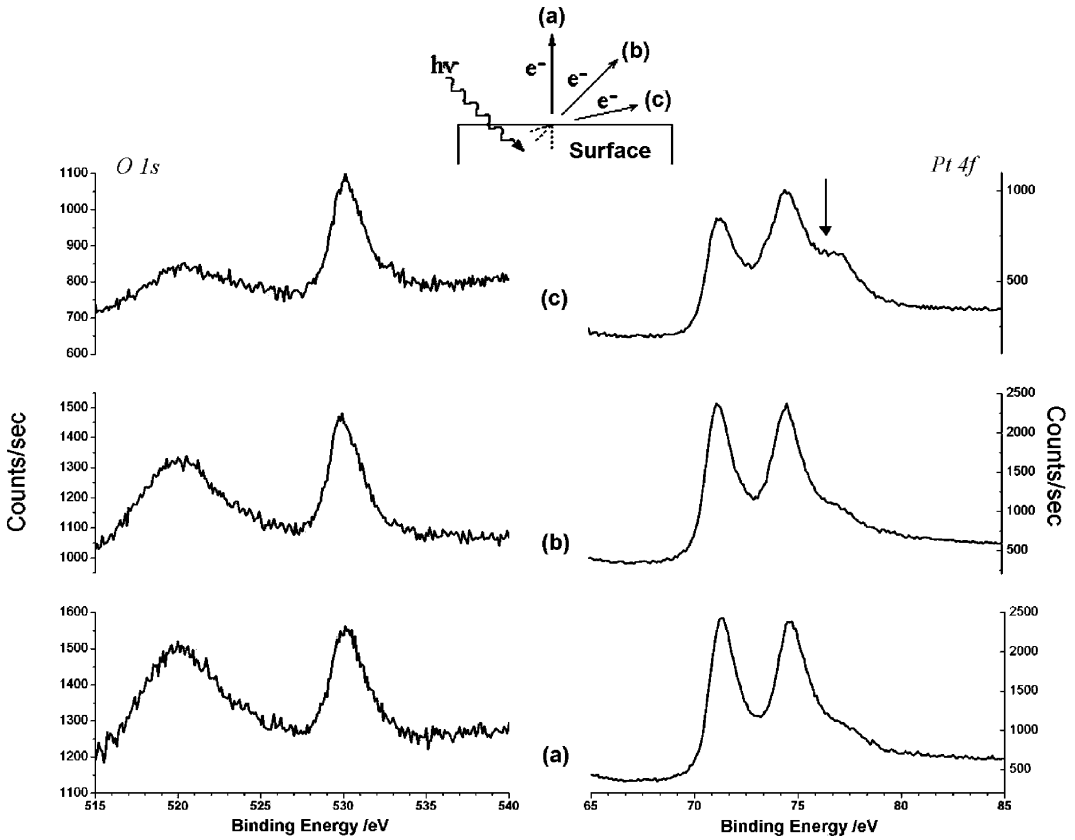

Fig. 5. Angle-resolved XPS spectra taken following exposure of the clean Pt(1 1 1) surface to 50 L atomic oxygen. XPS spectra were taken at normal emission (a), 45° (b) and 75° (c) off normal as detailed in the inset.

X-ray beam. Adlayer degradation was observed during long XPS acquisition times. For the longest acquisition times (~2 h) adlayer degradation was estimated to be ~6% by comparing O 1s peak intensities at the start and at the end of the series of scans. Analysis of the angle-resolved spectra reveals that there is a dramatic enhancement of emission from the O 1s and Pt 4f shoulder peaks at glancing take-off angles compared to the normal take-off angle. Since an enhancement of the surface sensitivity is expected at glancing take-off angles it is possible to conclude that the high concentration oxygen state does not exhibit significant bulk penetration. However, some surface penetration of oxygen by an exchange mechanism of the Pt atoms in the first two atomic layers can not be ruled out. Indeed the binding energy shifts in the Pt 4f spectrum suggest the formation of a strong Pt–O interaction.

3.2.3. Nature of the high coverage oxygen species

By comparing the O 1s and Pt 4f core level binding energies to those in the literature it is possible to comment on the chemical state and the interaction of the high coverage O species with Pt. Table 1 illustrates the various O 1s and Pt 4f binding energies for Pt and PtO_x compounds reported in the literature [32,33]. These values are compared to our measured values and show that the XPS data presented here is consistent with the formation of a Pt oxide. Indeed, further evidence for the formation of an oxide is provided by the high concentration of oxygen estimated from the relative XPS intensities. Oxygen chemi-

Table 1
Literature values for the binding energy of the Pt $4f_{7/2}$ and O 1s levels for Pt and Pt oxides

	Pt $4f_{7/2}$ (eV)	Pt $4f_{5/2}$ (eV)	O 1s (eV)	Reference
Pure Pt	71.2	74.5	/	[19]
$Pt_{(polycrystalline)}$ O	71.1	74.5	531.6, 530.0	[15]
Pt(1 1 1)–O-(2×2)	70.9	/	529.8	[11]
	71.2	74.5	530.2	[1]
	71.2	74.5	530.8	This work
PtO	72.3	/	530.5	[40]
$PtO_{2\ (bulk)}$	74.1	77.4	530.3	[1]
PtO_2 on Pt	71.2	74.5	530.2	[1]
High oxygen concentration Pt	73.5	76.8	530.2	This work

sorption on the Pt(1 1 1) surface usually ceases at lower coverages and does not provide a noticeable chemical shift of the substrate core levels [1,3–11].

It is well known that the chemisorption of electronegative adsorbates, like oxygen and carbon monoxide, can induce positive binding energy shifts of ≈1 eV [34]. For the work presented here, much larger shifts in the Pt 4f spectra, of the order of 2.3 eV, are observed for the high oxygen concentration state suggesting that a dramatic change in the chemical state of the Pt atoms has occurred. The formation of a Pt oxide, at least in part, seems a reasonable interpretation. The formation of an oxide necessitates charge transfer from the Pt to the oxygen, and results in the formation of cationic Pt atoms and anionic oxygen. Further evidence for the formation of a Pt oxide is evident from the stoichiometry of the shifted Pt 4f peak and the O $1s_{(530.2\,eV)}$ peak where an O:Pt ratio of 2.0 ± 0.5 was obtained, consistent with the formation of an oxide of the type PtO_2. However, Pt in PtO_2 is in the +4 oxidation state, but the Pt 4f binding energy shift observed in this work is not large enough to indicate Pt in this oxidation state. Conversely, the binding energy shift is larger than the binding energy shift expected for Pt in the +2 oxidation state (for PtO). Since the angle-resolved XPS indicates that the oxygen resides on or very close to the surface, a surface in the form of a chemisorbed oxygen layer, followed by a layer of Pt, a layer of O (either substitutional or interstitial), and then bulk Pt is tentatively proposed, shown schematically in Fig. 8 and discussed further in the CAICISS section. A structure such as this, with Pt in a +2 oxidation state, allows for both charge transfer and adsorbate electron withdrawing effects.

From the O 1s XPS spectra it is difficult to determine unambiguously the chemical state of the oxygen on the Pt surface. Binding energies referenced to the Fermi level for oxygen on metal surfaces are not unambiguously correlated to the chemical state of oxygen. For example, for oxygen on aluminium a transition from the chemisorbed state to oxidic state causes a shift in the O 1s level to a higher binding energy, while in contrast, the same transition for oxygen on nickel results in a shift to a lower binding energy. However, oxygen in an oxidic state has been characterised by an O 1s binding energy of 530.1 eV on Au(1 1 1) [29]; 530.8 eV on Ag(1 1 1) [35]; and 530.3 eV on Pd(1 1 1) [36]. The relatively low binding energy of the high concentration oxygen state is consistent for an O species with a formal oxidation state of −2 since it is known that, in general, the binding energy of core levels decrease as the number of valence electrons increase.

3.3. CAICISS observations

Low energy ion scattering using 3 keV He ions in a co-axial geometry (CAICISS) has been applied to the clean Pt(1 1 1) surface, the Pt–O high oxygen concentration surface, and to the Pt–O (2×2) surface obtained following annealing the high oxygen coverage surface at 500 °C. An analysis of the Pt CAICISS data and associated scattering simulations [23] has been used to distinguish

between the possible structural models for the Pt–O system. Only the CAICISS from the Pt atoms is presented in this study due to the low cross-section of oxygen, and its position on the low energy tail of the Pt peak.

CAICISS experiments were first carried out on the clean Pt(1 1 1) surface to test the experimental and simulation methodology. CAICISS incident angle scans were performed along the low index

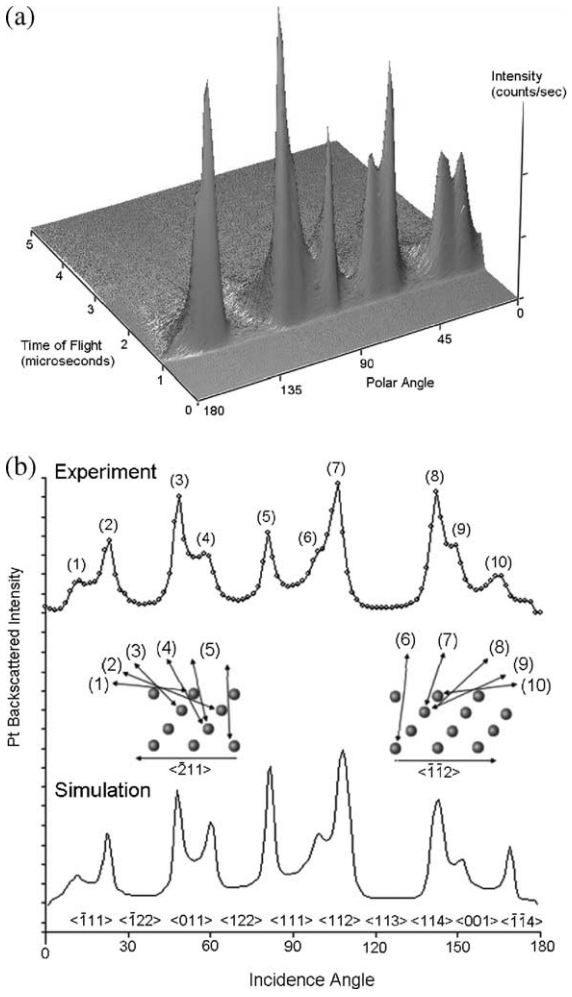

Fig. 6. (a) 3D plot of backscattered He^+ ion intensity as a function of time-of-flight from the Pt(1 1 1) surface for the full 180° polar scan along the ⟨2 1 1⟩ direction. (b) Plot of the experimental Pt backscattered ion intensity (upper spectrum) and simulated Pt backscattered ion intensity (lower spectrum) as a function of incidence angle in the ⟨2 1 1⟩ azimuth.

⟨2 1 1⟩ direction. In this geometry atoms of each atomic layer are contained within planes normal to the sample surface. Fig. 6a shows a 3d plot of backscattered ion intensity over a 20 μs TOF range versus ion incidence angle in the ⟨2 1 1⟩ direction. Fig. 6b shows a plot of the experimental Pt signal (at ~8 μs) scattering ion intensity (upper spectrum) and simulated Pt scattering ion intensity (lower spectrum) as a function of incidence angle in the ⟨2 1 1⟩ direction. This data shows a number of features, labelled 1–10, that are well reproduced in terms of incident angle position and intensity by the scattering simulations. The inset in Fig. 6 shows the scattering geometry for the incident angle scan along the ⟨2 1 1⟩ direction. Referenced to the experimental data the arrows on the inset indicate the incident angles at which a high intensity is to be expected due to shadow cone focusing [37].

3.3.1. CAICISS of the high oxygen concentration state

For the structural investigation of the high oxygen concentration state the surface was prepared by exposing the clean Pt(1 1 1) surface to 50 L of atomic oxygen. XPS was carried out to confirm the presence of Pt in the high oxidation state prior to CAICISS. CAICISS plots were taken along the ⟨2 1 1⟩ azimuth as a function of scattering angle for the clean Pt(1 1 1) surface, the high oxygen concentration Pt(1 1 1) surface, and the Pt–O (2×2) surface formed by heating the high oxygen concentration surface. For comparison the spectra from each of these surfaces are shown together in Fig. 7 over the incident angle range 0–180° (a), and 0–45° (b). The first feature to note is that there are significant differences between the three data sets in the early stages of acquisition (Fig. 7b) indicating that there have been significant changes in the overall surface structure. The second feature to note is that after a scattering angle of approximately 70° has been reached, or ≈1.5 h of acquisition, the data sets start to converge onto the clean Pt(1 1 1) spectrum. Furthermore, following the acquisition of the CAICISS data the XPS revealed that most of the oxygen was no longer present on the surface. Ion stimulated desorption (ISD) is suspected in this case for the loss of

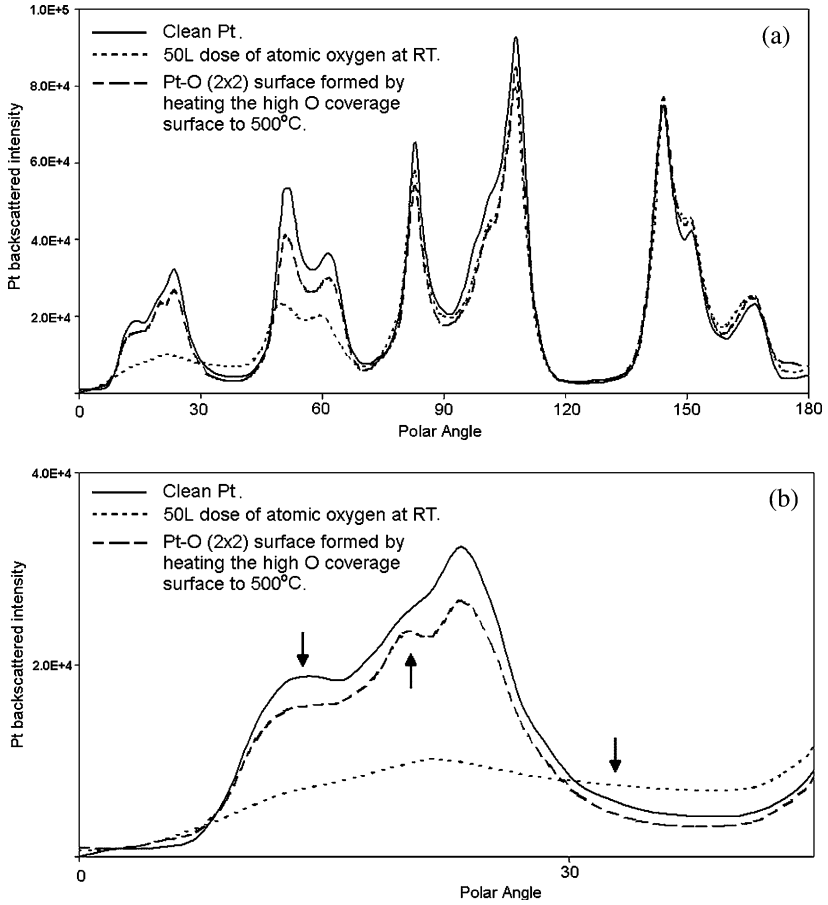

Fig. 7. CAICISS plots along the ⟨2 1 1⟩ azimuth as a function of scattering angle for the clean Pt(1 1 1) surface (a), the high oxygen concentration Pt(1 1 1) surface (b), and the Pt–O(2×2) surface formed by heating the high oxygen concentration surface (c).

oxygen from the surface region. The mechanism by which the conversion of the primary ion's potential energy into kinetic and potential energy of the desorbing species is an open question [38], however it is understood to result from an intra-atomic Auger decay process. Since exposure to 3 keV He ions results in the loss of most of the oxygen from the Pt surface (as evidenced by XPS), it can be concluded that the oxygen associated with the Pt 4f binding energy shift is on or near the surface in such a geometry as to be susceptible to ISD.

Within CAICISS the penetration depth of 3 keV He ions is limited to the top 3–4 atomic layers. As a result of ISD the analysis and simulation of the CAICISS spectra for this system was limited to the first 60° of the full polar scan. For these angles a slight misalignment in the axis of rotation of the sample face relative to the fixed ion beam was introduced so for each angle step (1.8°), the ion beam impinges on a different area of the sample. At these angles damage time to the Pt–O surface is limited to ~2 min.

The angle-resolved XPS data suggests (and the ISD implies) that for the Pt(1 1 1) surface exposed to a saturation dose of atomic oxygen at 25 °C, all the oxygen resides on or close to the surface with a concentration of approximately 2×10^{15} atoms cm^{-2}, and is partly in the form of an oxide. Accordingly, two models for the high oxygen

concentration surface have been simulated using the CAICISS simulation software:

1. *Interstitial*: The incorporation of oxygen in octahedral interstitial sites between the first and second Pt layers along with the adsorption of oxygen in threefold hollow sites.
2. *Substitutional*: The adsorption of oxygen in the second Pt layer by substitution with Pt, along with the adsorption of oxygen in threefold hollow sites.

It has been postulated that a critical coverage of adsorbed oxygen is required before the formation of a sub-surface oxygen can commence [16]. The simulations carried out here have assumed this critical coverage to be 0.5 ML, and confined O solely to the occupation in threefold hollow sites. Justification for this high critical coverage arises due to the fact that the formation of an oxide on the Pt(1 1 1) surface has not been observed for coverages up to 0.5 ML via other methods.

Fig. 8 shows the experimental data for the Pt scattering peak intensity as a function of the incidence of angle along the ⟨2 1 1⟩ azimuth, and the results of simulations based on the models described above, including schematics for the simulated structures. An adequate simulation for the high oxygen concentration state was not found, in particular the relative intensities (or lack of) in the backscattered Pt peaks could not be well reproduced in the simulations and the lack of intensity acted to hinder peak position determination. On the other hand, the lack of backscattered Pt intensity may indicate a lack of order within the near surface region. This would be in agreement with the LEED observations presented earlier. However, another possible explanation regards the homogeneity of the surface and, to this extent island growth of oxide domains can not be excluded. The results of the simulations do however appear to favour the substitutional adsorption of oxygen in the second Pt layer rather than the incorporation of oxygen within the octahedral sites. The feature labelled (I) in the substitutional adsorption model simulation is observed, albeit much broader and at a slightly higher angular position in the experimental data, although the lack of intensity and observed width of the peak precludes accurate determination of the peak position. The CAICISS simulations present evidence to favour substitutional type adsorption of Pt by O in at least the second Pt layer over interstitial adsorption of O.

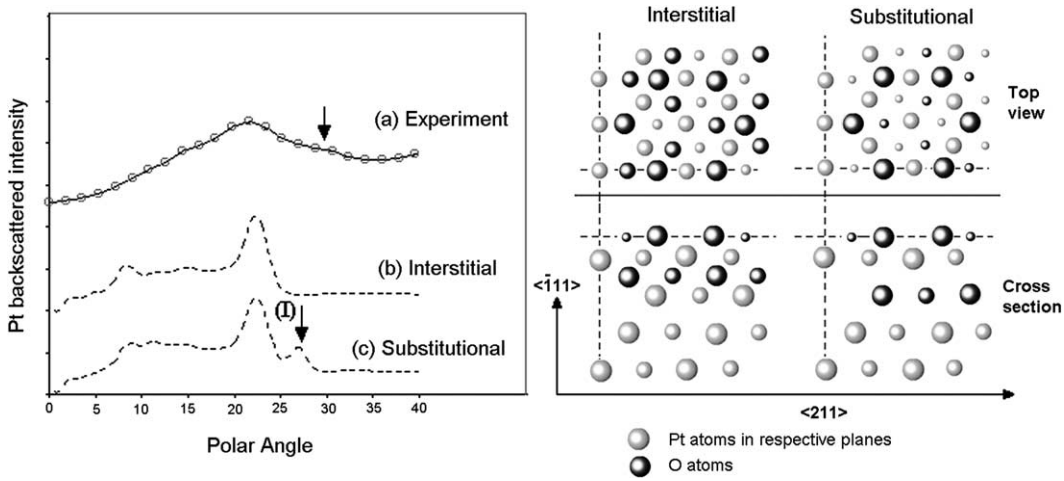

Fig. 8. Experimental data for the Pt scattering peak intensity as a function of the incidence of angle along the ⟨2 1 1⟩ azimuth for the Pt(1 1 1) surface exposed to 50 L atomic oxygen at 25 °C (a). The results of simulations based on the two proposed structures, shown in the inset; for interstitial (b) and substitutional incorporation (c) of O are shown.

3.3.2. CAICISS of the p(2 × 2)-O overlayer

The p(2×2)-O overlayer was prepared by annealing an atomic oxygen dosed surface at 500 °C for 20 min, and was confirmed using LEED and XPS. Based on a coverage of 0.25 ML, and from the known structure of the p(2×2)-O surface formed via low temperature molecular oxygen dosing followed by thermal activation [1,3–11,26–28], simulations for O occupying the f.c.c. site were carried out using structural parameters obtained from a LEED IV study by Somorjai and coworkers [27]. Fig. 9 spectrum (a) shows the experimental data for the Pt scattering peak intensity as a function of the incidence of angle along the ⟨2 1 1⟩ azimuth for the p(2×2)-O–Pt system obtained following annealing an atomic oxygen dosed surface. Fig. 9 spectrum (b) shows the result of a simulation conducted for the f.c.c. p(2×2)-O–Pt system using the known lattice parameters for this system. Whilst this simulation does not differ greatly from the experiment there are some notable features in the experimental data that are not reproduced in the f.c.c. simulation. The feature labelled I at grazing incidence on the experimental data in Fig. 9 spectrum (a) is not reproduced in the f.c.c. simulation. Further simulations were therefore carried out to explore the possibility of h.c.p. site occupation following the decomposition of the high concentration oxygen state. Recently, it has been shown that on exposing the Ru(1 1 1) surface to molecular oxygen at elevated temperatures the formation of sub-surface oxygen species is observed, and furthermore, *on*-surface oxygen *switches* from its normal f.c.c. site to the h.c.p. site [39]. Fig. 9 spectrum (c) shows the result of a simulation conducted for h.c.p. site occupation for the p(2×2)-O–Pt. At grazing incidence the feature labelled I on the experimental data is reproduced well in terms of position and intensity in the h.c.p. simulation (feature labelled II). However, there is also a feature in the h.c.p. simulation that is not resolved in the higher angle CAICISS data, at ≈53°, and labelled III on the figure. The absence of this feature may be due to the effect of ISD described earlier, however experiments aimed at minimising this effect, such as a lower ion dose and the accumulation of the full angular range within sections did not provide data to further support h.c.p. site occupation, although the deterioration in the surface was still noted following each angular section at a lower ion dose. While not conclusive the simulations appear to favour oxygen occupancy in the h.c.p. sites over the f.c.c. sites. Additionally, since the two sites have similar

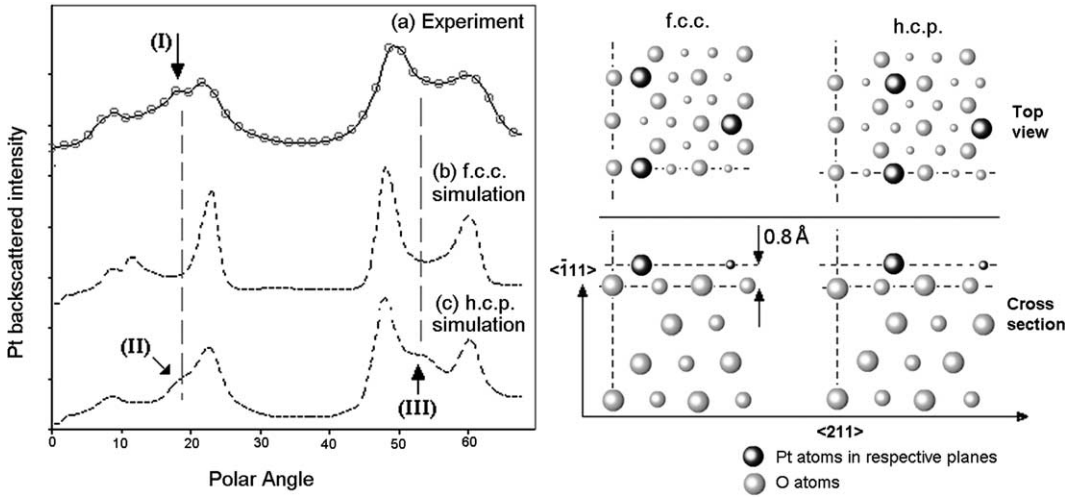

Fig. 9. Experimental data for the Pt scattering peak intensity as a function of the incidence of angle along the ⟨2 1 1⟩ azimuth for the (2×2)-O–Pt system obtained following annealing the Pt(1 1 1) surface exposed to 50 L atomic oxygen at 25 °C. The results and schematics of two proposed models used in the simulation software are also shown.

adsorption energies mixed site occupancy can not be ruled out.

4. Conclusions

In contrast to exposing a Pt(1 1 1) surface to molecular oxygen at room temperature, exposing a Pt(1 1 1) surface to externally generated thermally cracked atomic oxygen provides a pathway to an oxygen saturation coverage of greater than 0.25 ML. Both XPS and CAICISS data provide evidence for the formation of a sub-surface oxide at room temperature. The formation of such an oxide implies that the coverage of oxygen on the Pt surface via the external atomisation route exceeds the critical coverage at which the transition between the chemisorbed phase and the oxide film becomes thermodynamically and not kinetically determined. Detailed analysis of the CAICISS data and simulations suggest that this oxide state is formed by substitutional incorporation of O in the second Pt layer along with O adsorption in the surface hollow sites. On annealing at 500 °C the sub-surface oxide is lost and a p(2×2)-O reconstruction is observed. Grazing incidence CAICISS data and simulations for this annealed system favour oxygen occupancy in h.c.p. hollow sites over f.c.c. hollow sites, contrary to the adsorption geometry for O on the Pt(1 1 1) surface obtained via low temperature adsorption and thermal activation of molecular oxygen. However, the CAICISS data is not conclusive since a feature at a polar angle of 53° in the h.c.p. simulation is not resolved in the CAICISS data.

Acknowledgements

Marc Walker thanks the EPSRC for DTA Studentship. Rob Johnston is thanked for technical support.

References

[1] M. Peuckert, H.P. Bonzel, Surf. Sci. 145 (1984) 239.
[2] T. Engel, G. Ertl, in: D.A. King, D.P. Woodruff (Eds.), The Chemical Physics of Solid Surfaces and Heterogeneous Catalysis, vol. 4, Elsevier, Amsterdam, 1982 (Chapter 3).
[3] P.R. Norton, in: D.A. King, D.P. Woodruff (Eds.), The Chemical Physics of Solid Surfaces and Heterogeneous Catalysis, vol. 4, Elsevier, Amsterdam, 1982 (Chapter 2).
[4] J.L. Gland, B.A. Sexton, G.B. Fisher, Surf. Sci. 95 (1980) 587.
[5] J.L. Gland, Surf. Sci. 93 (1980) 487.
[6] P.R. Norton, Surf. Sci. 47 (1975) 98.
[7] D.H. Parker, M.E. Bartram, B.E. Koel, Surf. Sci. 217 (1989) 489.
[8] G. Lindauer, P. Légaré, G. Maire, Surf. Sci. 126 (1983) 301.
[9] G.N. Derry, P.N. Ross, Surf. Sci. 140 (1984) 165.
[10] H. Steininger, S. Lehwald, H. Ibach, Surf. Sci. 123 (1982) 1.
[11] C. Puglia, A. Nilsson, B. Hernnäs, O. Karis, P. Bennich, N. Mårtensson, Surf. Sci. 342 (1995) 119.
[12] D. Dahlgren, J.C. Hemminger, Surf. Sci. 123 (1982) L739.
[13] T. Matsushima, D.B. Almy, J.M. White, Surf. Sci 67 (1977) 89.
[14] H. Niehus, G. Comsa, Surf. Sci. 93 (1980) L147.
[15] P. Légaré, L. Hilaire, G. Maire, Surf. Sci. 141 (1984) 604.
[16] C.I. Carlisle, T. Fujimoto, W.S. Sim, D.A. King, Surf. Sci. 470 (2000) 15.
[17] M.V. Ganduglia-Pirovano, M. Scheffler, Phys. Rev. B 59 (1999) 15533.
[18] M. Todorova, W.X. Li, M.V. Ganduglia-Pirovano, C. Stampfl, K. Reuter, M. Scheffler, Phys. Rev. Lett. 89 (2002) 96103.
[19] J. Chastain, R.C. King Jr. (Eds.), Handbook of X-ray Photoelectron Spectroscopy, Physical Electronics, Eden Prairie, 1995.
[20] T.C.Q. Noakes, D.A. Hutt, C.F. McConville, D.P. Woodruff, Surf. Sci. 372 (1997) 117.
[21] H. Niehus, M. Voetz, C. Achete, K. Morgenstern, G. Comsa, in: R.J. MacDonald, E. Taglauer, K. Wandelt (Eds.), Surface Science, Principles and Current Applications, Springer, 1996, p. 38.
[22] W. Wach, K. Wittmaack, Nucl. Instrum. Methods 228 (1984) 1.
[23] H. Niehus, FAN simulation software, Humboldt-Universität zu Berlin, Institut für Physik, Berlin (http://asp2.physik.hu-berlin.de/).
[24] C.T. Campbell, G. Ertle, H. Kuipers, J. Segner, Surf. Sci. 107 (1981) 220.
[25] Oxford Applied Research, TC50 Thermal Gas Cracker http://www.oarersearch.co.uk.
[26] K. Mortensen, C. Klink, F. Jensen, F. Besenbacher, I. Stensgaard, Surf. Sci. 220 (1989) L701.
[27] N. Materer, U. Starke, A. Barbieri, R. Döll, K. Heinz, M.A. Van Hove, G.A. Somorjai, Surf. Sci. 325 (1995) 207.
[28] S. Paavilainen, J.A. Nieminen, Surf. Sci. 521 (2002) 69.
[29] N. Saliba, D.H. Parker, B.E. Koel, Surf. Sci. 410 (1998) 270.
[30] A.G. Sault, R.J. Madix, Surf. Sci. 169 (1986) 347.
[31] A.F. Carley, M.W. Roberts, Proc. Roy. Soc. London A 363 (1978) 403.
[32] T.L. Barr, J. Phys. Chem. 82 (1978) 1801.
[33] D. Briggs, M.P. Seah (Eds.), Practical Surface Analysis, vol. 1, 2nd ed., J. Wiley and Sons, 1993.

[34] G. Apai, R.C. Baetzold, E. Shustorovich, R. Jaeger, Surf. Sci. 116 (1982) L191.
[35] S.R. Bare, K. Griffiths, W.N. Lennard, H.T. Tang, Surf. Sci. 342 (1995) 185.
[36] B.A. Banse, B.E. Koel, Surf. Sci. 232 (1990) 275.
[37] H. Niehus, W. Heiland, E. Taglauer, Surf. Sci. Rept. 17 (4/5) (1993) 213.
[38] R. Souda, Int. J. Mass Spectrom. 202 (2000) 199.
[39] M.V. Ganduglia-Pirovano, K. Reuter, M. Scheffler, Phys. Rev. B 65 (2002) 245426.
[40] M.-C. Jung, H.-D. Kim, M. Han, W. Jo, D.C. Kim, Jpn. J. Appl. Phys. 38 (1999) 4872.
[41] H.P. Bonzel, A.M. Franken, G. Pirug, Surf. Sci. 104 (1981) 625.